Journal of Catalysis 357 (2018) 80–89

Contents lists available at ScienceDirect

Journal of Catalysis

journal homepage: www.elsevier.com/locate/jcat

Isomerisation of *n*-hexane over bifunctional Pt-heteropoly acid catalyst: Enhancing effect of gold

Abdulrahman Alazman, Domagoj Belic, Elena F. Kozhevnikova, Ivan V. Kozhevnikov *

University of Liverpool, Department of Chemistry, Liverpool L69 7ZD, UK

ARTICLE INFO

Article history:
Received 21 September 2017
Revised 30 October 2017
Accepted 2 November 2017

Keywords:
Isomerisation
n-Hexane
Bifunctional catalysis
Platinum
Gold
Heteropoly acid

ABSTRACT

Isomerisation of *n*-hexane was studied in the presence of acid and bifunctional metal-acid catalysts based on Keggin-type heteropoly acids (HPA), in particular focusing on $Cs_{2.5}H_{0.5}PW_{12}O_{40}$ (CsPW) and Pt/CsPW as the catalysts, using a fixed-bed microreactor under differential conditions (*n*-hexane conversion ≤ 10%) at 180–220 °C, ambient pressure and a ratio of *n*-hexane and H_2 partial pressures of 0.06–0.24. The turnover rate of HPA-catalysed isomerisation was found to correlate with the acid strength of HPA (initial enthalpy of ammonia adsorption). Bifunctional Pt-HPA catalysts were more efficient than monofunctional HPA catalysts. In the isomerisation over Pt/CsPW bifunctional catalyst, *n*-hexane dehydrogenation step was found to equilibrate at a molar ratio of Pt and H^+ surface sites $Pt_s/H^+ \geq 0.8$, corresponding to a Pt loading ≥6%. Bimetallic PtAu/CsPW catalyst showed higher activity in *n*-hexane isomerisation than Pt/CsPW, although the Au alone without Pt was inert. In the presence of Au, the turnover rate at Pt sites increased more than twofold. The effect of Au is attributed to PtAu alloying. Scanning transmission electron microscopy–energy dispersive X-ray spectroscopy (STEM-EDX) and X-ray diffraction (XRD) analyses of PtAu/CsPW indicated the presence of bimetallic PtAu nanoparticles with a wide range of Pt/Au atomic ratios.

1. Introduction

Isomerisation of linear C_5–C_6 alkanes, which are relatively stable toward cracking, is used in industry to produce high octane gasoline. For example, *n*-hexane isomerisation to 2-methylpentane (2MP) and 3-methylpentane (3MP) increases the research octane number (RON) from 25 to 74. Further branching to 2,2- and 2,3-dimethylbutane isomers (22DMB and 23DMB) increases RON to 96 and 105, respectively [1].

Alkane isomerisation can occur via an acid-catalysed pathway on strong Lewis and Brønsted acid sites [2,3] (Scheme 1). With Lewis acids, a linear alkane, e.g., *n*-hexane, can be isomerised through a monomolecular carbenium-ion chain mechanism including carbenium ions produced by H^- abstraction on Lewis acid sites. The carbenium ions then form a protonated cyclopropane intermediate, which undergoes β-migration of methyl group followed by H^- transfer from an *n*-hexane molecule to give mono-branched 2MP and 3MP as the primary isomerisation products together with the carbenium ions continuing the chain process (not shown in Scheme 1). Subsequent isomerisation of 2MP and 3MP can lead to formation of 23DMB and 22DMB. On strong Brønsted acid sites, carbonium ions are formed by protonation of a C—H bond. The carbonium ions then undergo H_2 elimination to give the carbenium ions leading to the formation of 2MP and 3MP. Proton elimination from the carbenium ions could give alkenes. The latter form oligomers and coke, which cause catalyst deactivation (Scheme 1). In addition, C_{6-} hydrocarbons can be formed by cracking of hexane isomers. Also C_{6-} and C_{6+} products can be produced by disproportionation of C_{12} cation intermediates formed from the C_6 carbenium ions and an alkene (bimolecular mechanism) [2,3].

Industrial isomerisation of linear alkanes is carried out using bifunctional metal-acid catalysts, usually platinum supported on chlorinated alumina or acidic zeolites (e.g., mordenite) in the presence of hydrogen (hydroisomerisation) [1]. The reaction is suggested to proceed in accordance with Scheme 2 involving alkane dehydrogenation on Pt sites followed by isomerisation of the alkene formed on acid sites of support [4]. The alkene isomer is then hydrogenated on the platinum to give the branched alkane. The bifunctional pathway (Scheme 2) is much more efficient than the acid-catalysed pathway (Scheme 1). Platinum in the bifunctional catalyst is important not only in enhancing the isomerisation process, but also in reducing the steady state alkene concentration. The latter increases reaction selectivity due to diminishing the con-

* Corresponding author.
E-mail address: kozhev@liverpool.ac.uk (I.V. Kozhevnikov).

https://doi.org/10.1016/j.jcat.2017.11.001
0021-9517/

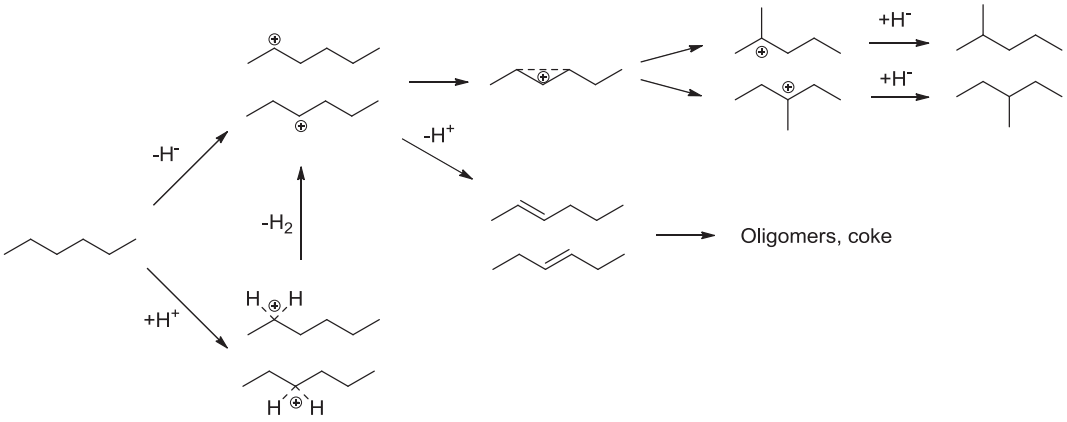

Scheme 1. Acid-catalysed pathway for *n*-hexane isomerisation via monomolecular mechanism.

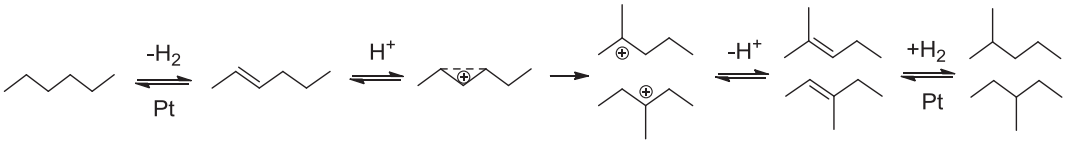

Scheme 2. Bifunctional catalysed pathway for *n*-hexane isomerisation (hydroisomerisation).

tribution of the bimolecular mechanism [5] and reduces coke formation, thus improving catalyst lifetime [1].

Heteropoly acids (HPAs) possessing very strong Brønsted acidity have attracted much interest as acid catalysts, in particular tungsten HPAs with Keggin structure such as $H_3PW_{12}O_{40}$ (HPW) and $H_4SiW_{12}O_{40}$ (HSiW) [6–8]. In recent years, Pt-HPA bifunctional catalysis for alkane isomerisation has been studied extensively to show its high efficiency in this reaction ([9–12] and references therein).

Here, we investigate the Pt-HPA bifunctional catalysis in the isomerisation of *n*-hexane, focussing on the use of $Cs_{2.5}H_{0.5}PW_{12}O_{40}$ (CsPW) as the acid component. CsPW is an insoluble acidic salt of 12-tungstophosphoric acid, which has important advantages over the parent HPW in possessing much larger surface area (hence larger surface acidity) and higher thermal stability, while having the Brønsted acid sites almost as strong as in HPW [6,7]. Also, we report here an enhancing effect of Au on *n*-hexane isomerisation over Pt/CsPW. It is demonstrated that modification of the Pt/CsPW catalyst with gold increases the reaction turnover rate at Pt surface sites more than twofold, although the gold alone without Pt is practically inactive in this reaction. It is suggested that the enhancement is caused by PtAu alloying. STEM-EDX and XRD analysis of the PtAu/CsPW catalysts indicates the presence of bimetallic PtAu nanoparticles with a wide range of Pt/Au atomic ratios.

2. Experimental

2.1. Chemicals and catalysts

n-Hexane (>99%), H_2PtCl_6 hydrate, $HAuCl_4{\cdot}3H_2O$, $H_3PW_{12}O_{40}$ (HPW, 99%) and $H_4SiW_{12}O_{40}$ (HSiW, 99.9%) hydrates were all purchased from Sigma-Aldrich. Catalyst supports P25 titania (anatase/rutile = 3:1) and Aerosil 300 silica were from Degussa. H_2 gas cylinders (>99%) were supplied by the British Oxygen Company.

Cesium tungstophosphate $Cs_{2.5}H_{0.5}PW_{12}O_{40}$ (CsPW) was prepared according to the literature procedure [13,14] by adding drop-wise the required amount of aqueous solution of cesium carbonate to aqueous solution of $H_3PW_{12}O_{40}$ to afford CsPW as a white precipitate. The material was isolated, vacuum dried at 150 °C/10^{-3} kPa for 1.5 h. A similar procedure was used for the preparation of $Cs_{2.25}H_{0.75}PW_{12}O_{40}$ ($Cs_{2.25}$PW). Silica- and titania-supported HPW and HSiW catalysts were prepared by wet impregnation of HPA onto support as described elsewhere [14] and dried at 150 °C/10^{-3} kPa for 1.5 h. Information about these solid acid catalysts and supports is given in Table 1; it includes their texture, proton site density and acid strength represented by the initial enthalpy of ammonia adsorption [14].

CsPW-supported bifunctional metal-acid catalysts, Pt/CsPW and Au/CsPW, were prepared as described previously [15] by wet impregnation of CsPW powder with aqueous solutions of H_2PtCl_6 or $HAuCl_4$. This involved stirring the aqueous slurry at 50 °C for 2 h followed by rotoevaporation to dryness and reduction with H_2 flow at 250 °C for 2 h. The bimetallic PtAu/CsPW catalysts were prepared similarly by co-impregnation of CsPW with H_2PtCl_6 and $HAuCl_4$ with reduction by H_2 as above. Metal content in these catalysts was determined by ICP-AES analysis (see below). Physical mixtures of bifunctional catalysts and SiO_2 with a specified Pt and Au loading were prepared by grinding the catalysts with Aerosil 300 silica. Properties of the bifunctional catalysts are shown in Table 2.

2.2. Techniques

The surface area and porosity of catalysts were determined from nitrogen physisorption measured on a Micromeritics ASAP 2010 instrument at −196 °C. Before measurement, the samples were evacuated at 250 °C for 2 h. Powder X-ray diffraction (XRD) patterns of catalysts were recorded on a PANalytical Xpert diffractometer with CuKα radiation (λ = 1.542 Å) and attributed using the JCPDS database. Inductively coupled plasma atomic emission spectroscopy (ICP-AES) elemental analysis was carried out on a Spectro Ciros optical emission spectrometer. Thermo Flash EA 1112 analyser was used to determine carbon content in spent catalysts by combustion chemical analysis.

Scanning transmission electron microscopy (STEM) imaging and energy dispersive X-ray spectroscopy (EDX) analysis of catalysts was carried out on an aberration-corrected JEOL JEM

Table 1
Information about acid catalysts [14].

Catalysts	S_{BET}[a] $m^2 g^{-1}$	Pore volume[b] $cm^3 g^{-1}$	Pore size[c] Å	H^+ sites[d] mmol g^{-1}	ΔH_{NH3}[e] kJ mol^{-1}
TiO_2 (P25 Degussa)	44	0.10	90		
SiO_2 (Aerosil 300)	300[f]				
$H_3PW_{12}O_{40}$ (HPW)	5.6	0.04	81	0.019	−197
$H_4SiW_{12}O_{40}$ (HSiW)	9.0	0.02	71	0.042	−171
$Cs_{2.5}H_{0.5}PW_{12}O_{40}$ (CsPW)	132	0.10	29	0.076	−164
$Cs_{2.25}H_{0.75}PW_{12}O_{40}$	128	0.07	22	0.110	−162
15%HPW/SiO_2	202	1.00	169	0.156	−154
15%HSiW/SiO_2	221	1.02	185	0.208	−154
15%HPW/TiO_2	45	0.20	174	0.156	−143

[a] BET surface area.
[b] Single point total pore volume at $P/P_o = 0.97$.
[c] Average BET pore diameter.
[d] Proton site density (see the text for its calculation).
[e] Initial enthalpy of NH_3 adsorption at 150 °C (±3 kJ mol^{-1}).
[f] Manufacturer's value.

Table 2
Information about bifunctional catalysts.

Catalyst[a]	S_{BET}[b] $m^2 g^{-1}$	Pore volume[c] $cm^3 g^{-1}$	Pore size[d] Å	D[e]	d[f] nm
CsPW	132	0.10	29		
0.11%Pt/CsPW	125	0.101	30	0.85	1.1
0.23%Pt/CsPW	121	0.090	30	0.76	1.2
0.32%Pt/CsPW	124	0.095	31	0.61	1.5
0.71%Pt/CsPW	112	0.088	32	0.55	1.6
2.45%Pt/CsPW	110	0.085	31	0.29	3.1
3.56%Pt/CsPW	102	0.072	28	0.13	6.9
3.76%Pt/CsPW	108	0.078	29	0.26	3.5
5.78%Pt/CsPW	93	0.076	33	0.19	4.7
5.87%Pt/CsPW	102	0.067	26	0.22	4.1
11.5%Pt/CsPW	70	0.069	40	0.15	6.0
0.28%Pt/0.35%Au/CsPW	122	0.107	35	0.55	1.6
5.57%Pt/4.25%Au/CsPW	91	0.082	36	0.17	5.3
2.62%Au/CsPW[g]	103	0.090	35		≤10

[a] Metal loading obtained from ICP-AES analysis.
[b] BET surface area.
[c] Single point total pore volume at $P/P_o = 0.97$.
[d] Average BET pore diameter.
[e] Pt dispersion determined from H_2/O_2 titration; for PtAu catalysts assuming negligible H_2 adsorption on gold.
[f] Metal particle diameter: for Pt from the equation d (nm) = 0.9/D, for Au from STEM.
[g] No H_2 adsorption observed.

2100FCs instrument operated at 200 kV, equipped with an EDAX Octane T Optima 60 windowless silicon drift detector. For STEM analysis, the samples were prepared by scooping up the catalyst powder by a TEM grid (holey carbon film on 300 Ni mesh, Agar Scientific) followed by shaking to remove excess material from the grid.

Platinum dispersion in the catalysts was measured on a Micromeritics TPD/TPR 2900 instrument using the hydrogen-oxygen titration pulse method in a flow system at room temperature as described previously [15,16]. The Pt dispersion, D, defined as the Pt fraction at the surface, $D = Pt_s/Pt_{total}$, was calculated assuming the stoichiometry of H_2 adsorption: $Pt_sO + 1.5\ H_2 \rightarrow Pt_s\text{-}H + H_2O$ [17,18]. Adsorption of H_2 observed on the PtAu catalysts was attributed entirely to platinum as Au/CsPW did not adsorb any hydrogen under such conditions [15]. The average diameter of Pt particles, d, was obtained from the empirical equation d (nm) = 0.9/D [18]. For some PtAu/CsPW catalysts, the metal particle size was also estimated by XRD using the Scherrer equation, with line broadening assessed as the full width at half maximum intensity (FWHM).

2.3. Catalyst testing

Isomerisation of *n*-hexane was carried out at the gas-solid interface in flowing H_2 at 180–220 °C. The catalysts were tested under atmospheric pressure at a ratio of *n*-hexane and H_2 partial pressures of 0.06–0.24 in a Pyrex fixed-bed down-flow microreactor (9 mm internal diameter) fitted with an on-line gas chromatograph (Varian Star 3400 CX instrument with a 30 m × 0.25 mm HP INNOWAX capillary column and a flame ionisation detector). For more accurate off-line GC analysis of C_{6-} hydrocarbon products, a 60 m × 0.32 mm GS-GasPro capillary column was used. The temperature in the reactor was controlled by a Eurotherm controller (±0.5 °C) using a thermocouple placed at the top of the catalyst bed. *n*-Hexane was fed by passing H_2 flow controlled by a Brooks mass flow controller through a stainless steel saturator, which held *n*-hexane at 0 °C (ice bath) to maintain the chosen reactant partial pressure of 5.78 kPa (5.8 mol% concentration of *n*-hexane in H_2 flow) unless stated otherwise. The downstream gas lines and valves were heated to 150 °C to prevent substrate and product condensation. The gas feed entered the reactor from the top at a flow rate of 20 mL min^{-1}. The reactor was packed with 0.20 g catalyst powder of 45–180 μm particle size. Unless stated otherwise, the reaction was carried out at a space time $W/F = 69.2$ g h mol^{-1}, where W is the catalyst weight (in grams) and F is the inlet molar flow rate of *n*-hexane (in mol h^{-1}). Prior to reaction, the catalysts were pre-treated in situ for 1 h at the reaction temperature. Once reaction started, the downstream gas flow was analysed by the on-line GC to obtain reactant conversion and product composition. Product selectivity was defined as moles of product formed per one

mole of *n*-hexane converted and quoted in mole per cent. The mean absolute percentage error in conversion and selectivity was ≤5% and the carbon balance was maintained within 95%. Reaction rates (R) were determined as $R = XF/W$ (in mol g_{cat}^{-1} h^{-1}), where X is the fractional conversion of *n*-hexane. In most cases, the reaction was carried out at differential conditions ($X \leq 0.1$), where X is directly proportional to the reaction rate. In some cases, the catalysts were diluted with silica in order to achieve low conversion.

3. Results and discussion

3.1. Acid-catalysed isomerisation of n-hexane

Bulk and supported heteropoly acids HSiW and HPW were found to have small activity in *n*-hexane isomerisation. Bulk acidic Cs salts of HPW, i.e. CsPW and $Cs_{2.25}PW$, showed better activities in this reaction (Table 3) despite their weaker acidity compared to the bulk HPW (Table 1). This can be attributed to the larger surface area hence larger proton site density of the Cs salts (Table 1). 2MP and 3MP were the main reaction products, which formed with 65–67% and 29–31% selectivity, respectively, together with 3–5% of cracking products (mainly C_3–C_5 hydrocarbons). Double-branched 23DMB isomer was formed in less than 1% selectivity. Strong catalyst deactivation was observed, which can be assigned to coke deposition. Initially white, CsPW catalyst turned black after reaction, with a carbon content of 0.6 wt% as determined by combustion chemical analysis for the reaction at 180 °C after 6 h time on stream (Table S1 in the Supporting Information). As seen from the time course of reaction with CsPW at 200 °C (Fig. 1), *n*-hexane conversion is strongly affected by catalyst deactivation, however without changing reaction selectivity. Practically the same results were obtained when using N_2 instead of H_2 as the carrier gas.

Table 3
Acid-catalysed isomerisation of *n*-hexane.[a]

Catalyst	Conversion[b] %	10^3 R[c] mol g^{-1} h^{-1}	TOF_H[d] h^{-1}
CsPW	2.7	0.38	5.1
$Cs_{2.25}H_{0.75}PW_{12}O_{40}$ ($Cs_{2.25}PW$)	2.8	0.41	3.7
HPW	0.7	0.10	5.2
HSiW	1.0	0.15	3.6
15%HPW/SiO_2	0.34	0.049	0.32
15%HPW/TiO_2	0.14	0.020	0.13
15%HSiW/SiO_2	0.16	0.023	0.11

[a] 200 °C, 0.20 g catalyst, 5.78 kPa *n*-hexane partial pressure in H_2 flow (20 mL min^{-1}).
[b] *n*-Hexane conversion at 1 h time on stream (mean of two parallel runs).
[c] Reaction rate calculated from $R = XF/W$, where X is the fractional conversion of *n*-hexane, W is the catalyst weight (0.20 g) and F is the molar flow rate of *n*-hexane (W/F = 69.2 g h mol^{-1}).
[d] Turnover frequency per surface proton site; proton site densities are given in Table 1.

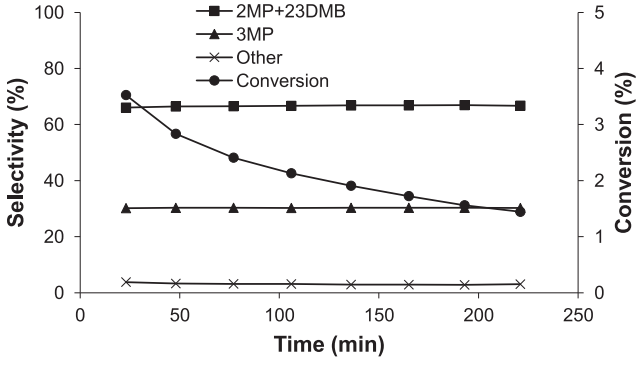

Fig. 1. Isomerisation of *n*-hexane catalysed by CsPW (0.20 g) at 200 °C, 5.78 kPa *n*-hexane partial pressure in H_2 flow (20 mL min^{-1}).

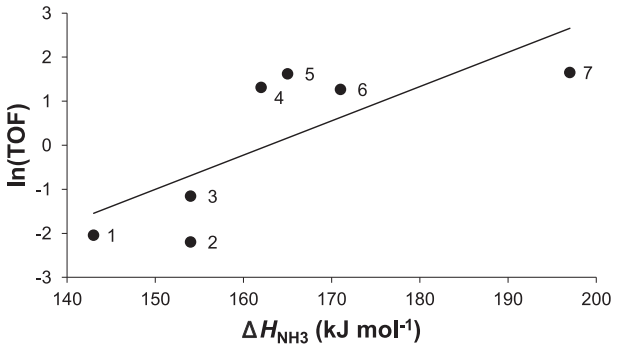

Fig. 2. Plot of ln(TOF) (TOF in h^{-1}) versus ΔH_{NH3} for *n*-hexane isomerisation catalysed by HPA catalysts (0.20 g catalyst, 200 °C, 5.78 kPa *n*-hexane partial pressure, 20 mL min^{-1} H_2 flow rate): 15%HPW/TiO_2 (1), 15%HSiW/SiO_2 (2), 15% HPW/SiO_2 (3), $Cs_{2.25}PW$ (4), CsPW (5), HSiW (6), HPW (7).

The rates of acid-catalysed isomerisation of *n*-hexane (R) and turnover frequencies (TOF_H) per surface proton site were calculated using the values of *n*-hexane conversion for 1 h time on stream (Table 3). The required densities of surface proton sites are given in Table 1; these were estimated as described elsewhere [14]. For supported HPA catalysts, which contained HPW or HSiW at a sub-monolayer loading of 15%, all HPA protons were assumed to be equally available for reaction. For bulk HPW, HSiW and Cs salts of HPW, the number of surface proton sites was calculated using a Keggin unit cross section of 144 $Å^2$ [6,7] and the catalyst surface areas from Table 1.

The TOF_H values obtained ranged from 0.1 h^{-1} for 15% HPW/TiO_2 to 5.2 h^{-1} for bulk HPW (Table 3) indicating a strong effect of catalyst acid strength on the reaction turnover rate. Fig. 2 shows the relationship between the activity of catalysts in *n*-hexane isomerisation, ln (TOF_H), and their acid strength represented by the initial enthalpy of ammonia adsorption, ΔH_{NH3} (Table 1). Although there is considerable scatter of points, which is probably caused by catalyst deactivation, this relationship clearly indicates that Brønsted acid sites play important role in *n*-hexane isomerisation over heteropoly acid catalysts as can be anticipated from the reaction mechanism shown in Scheme 1.

3.2. Bifunctional metal-acid catalysed isomerisation of n-hexane

As expected, Pt/CsPW bifunctional catalysts in the presence of H_2 were more efficient in *n*-hexane isomerisation than the acid catalyst CsPW. The Pt/CsPW catalysts showed higher catalytic activity and displayed much less catalyst deactivation compared to CsPW (Fig. 3). The amount of coke in spent Pt/CsPW catalysts was below the detection limit after reaction at 180 °C (6 h on stream) (Table S1). When using N_2 as the carrier gas in the absence of H_2, the activity of Pt/CsPW was much lower and strong catalyst deactivation was observed (Fig. S1). The activity of Pt/CsPW increased with increasing Pt loading (Table 4, entries 1–3, 5 and 6). Thus 5.78%Pt/CsPW gave a tenfold higher *n*-hexane conversion than CsPW at 200 °C (entries 2 and 6). The reaction products included 2MP (64–69% selectivity), 3MP (30–32%) and 23DMB (0.8–1.2%) together with 2–5% of cracking products (mainly C_3-C_5 hydrocarbons) at *n*-hexane conversion of 4–22%. Similar product selectivity was observed with CsPW without Pt (Table 4, entries 1 and 2). This indicates that Pt does not affect β-migration of methyl group in the protonated cyclopropane intermediate (Schemes 1 and 2). The low 23DMB selectivity can be explained by the low *n*-hexane conver-

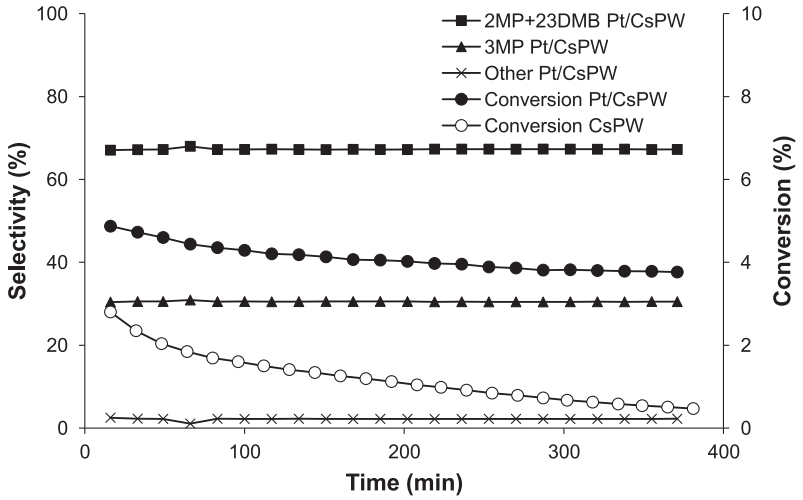

Fig. 3. Isomerisation of *n*-hexane catalysed by 0.32%Pt/CsPW (0.20 g) at 180 °C, 5.78 kPa *n*-hexane partial pressure in H_2 flow (20 mL min^{-1}). Open circles show *n*-hexane conversion with CsPW catalyst at the same conditions; reaction selectivities are similar in both cases.

Table 4
n-Hexane isomerisation over bifunctional metal-acid catalysts.[a]

Catalyst	Temperature (°C)	Conversion[b] (%)	Selectivity[c] (%)		
			2MP + 23DMB[d]	3MP	Other[e]
(1) CsPW	180	1.5 (4)	68.6	31.1	0.3
(2) CsPW	200	2.2 (4)	66.9	30.4	2.7
(3) 0.32%Pt/CsPW	180	3.9 (6)	65.9	31.6	2.5
(4) 5.78%Pt/CsPW	150	1.5 (2)			
(5) 5.78%Pt/CsPW	180	8.0 (6)	65.8	32.0	2.2
(6) 5.78%Pt/CsPW	200	22.3 (4)	64.0	31.9	4.1
(7) 0.28%Pt/0.35%Au/CsPW	180	6.6 (6)	66.8	30.7	2.5
(8) 5.57%Pt/4.25%Au/CsPW	180	10.2 (6)	64.1	34.9	1.0
(9) 2.62%Au/CsPW	180	1.4 (4)	65.1	30.4	4.6
(10) 2.62%Au/CsPW	180	1.3 (6)	65.1	30.4	4.6

[a] 0.20 g catalyst, 5.78 kPa *n*-hexane partial pressure in H_2 flow (20 mL min^{-1}).
[b,c] Average *n*-hexane conversion and product selectivity over the time on stream given in square brackets.
[d] 2,3-Dimethylbutane (23DMB) selectivity 0.8–1.2%.
[e] C_{6-} cracking products, mainly C_3–C_5; no C_{6+} hydrocarbons observed.

sion under the chosen differential reaction conditions. It should be noted that the conversions and selectivities observed were far from equilibrium values. The equilibrium C_6 alkane isomer mixture at 200 °C contains *n*-hexane (14%), 2MP (31%), 3MP (20%), 22DMB (26%) and 23DMB (9%), which corresponds to 86% *n*-hexane conversion [19]. It should be noted that there was no C_{6+} hydrocarbons observed among the reaction products. This indicates the reaction occurring via the monomolecular mechanism (Scheme 2) in agreement with the literature [5].

Kinetics of alkane isomerisation over Pt-acid bifunctional catalysts based on zeolites and heteropoly acids has been addressed in previous reports [10,20,21]. *n*-Hexane is relatively stable towards cracking, therefore the rate of isomerisation could be approximated by the rate of *n*-hexane conversion [21]. When the dehydrogenation reaction step is equilibrated and the isomerisation step is rate limiting (Scheme 2) and also the hydrocarbon concentrations inside catalyst pores are in equilibrium with the gas phase, the overall rate of isomerisation *R* is given by Eq. (1), where K_d is the equilibrium constant of dehydrogenation, K_p is the equilibrium constant of protonation, k_i is the rate constant of isomerisation, P_{C6} is the partial pressure of *n*-hexane, p_{H2} is the partial pressure of hydrogen and α is the order of reaction ($\alpha \leq 1$) [20,21].

$$R = k_i \frac{K_d K_p \left(\frac{P_{C_6}}{P_{H_2}}\right)}{1 + K_d K_p \left(\frac{P_{C_6}}{P_{H_2}}\right)} \approx k_i \left(K_d K_p \frac{P_{C_6}}{P_{H_2}}\right)^{\alpha} \quad (1)$$

The rate limiting step is determined by the balance between metal and acid functionalities in bifunctional catalyst, i.e., the ratio of accessible surface metal and acid sites Pt_s/H^+ [4,10,20–22]. In the case of catalysts based on zeolites (e.g., H-MOR, H-BEA, H-USY, etc.), the dehydrogenation step is usually equilibrated at $Pt_s/H^+ < 0.1$, and the isomerisation step becomes rate limiting [20,22]. For Pt-HPA catalysts based on HPW possessing significantly stronger proton sites compared to zeolites [14], a much higher Pt_s/H^+ ratio may be required to equilibrate the dehydrogenation step [10].

Fig. 4 shows the plot of *n*-hexane conversion over Pt/CsPW catalyst as a function of Pt loading. As seen, the conversion increases with increasing the Pt loading, levelling off at ≥6% Pt loading. Fig. 5 shows the same results represented as turnover frequencies TOF_H and TOF_{Pt} versus the Pt_s/H^+ ratio, where the TOF_H and TOF_{Pt} were calculated per surface H^+ and Pt_s site, respectively, using conversion data at 200 °C and the Pt dispersion from Table 2. It was also assumed that the proton site density of CsPW (0.076 mmol g^{-1}, Table 1) was not affected by Pt loading. The contribution of CsPW (Table 4, entry 2) was subtracted from the total conversion when calculating the TOF_{Pt}. As expected from Scheme 2, TOF_H increases and TOF_{Pt} decreases with increasing the Pt_s/H^+ ratio, levelling off as the dehydrogenation step reaches quasi-equilibrium (Fig. 5). These results demonstrate that under the chosen reaction conditions (200 °C, $P_{C6}/p_{H2} = 0.061$), *n*-hexane dehydrogenation step is equilibrated over Pt/CsPW catalyst at $Pt_s/H^+ \geq 0.8$, which corresponds to a Pt loading of ~6%. This Pt_s/H^+ value is predictably

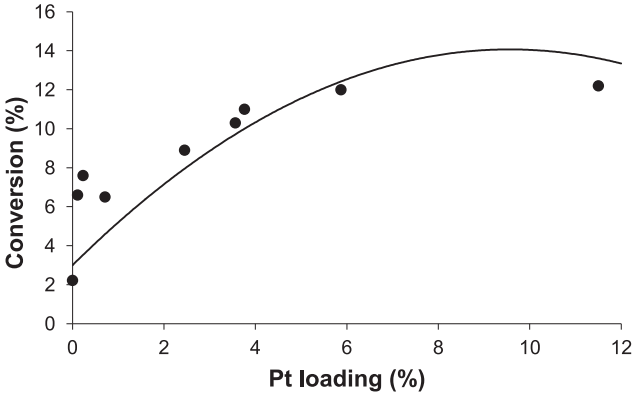

Fig. 4. Plot of *n*-hexane conversion versus Pt loading: Pt/CsPW (0.20 g), 200 °C, 5.78 kPa *n*-hexane partial pressure in H_2 flow (20 mL min^{-1}), 5 h time on stream.

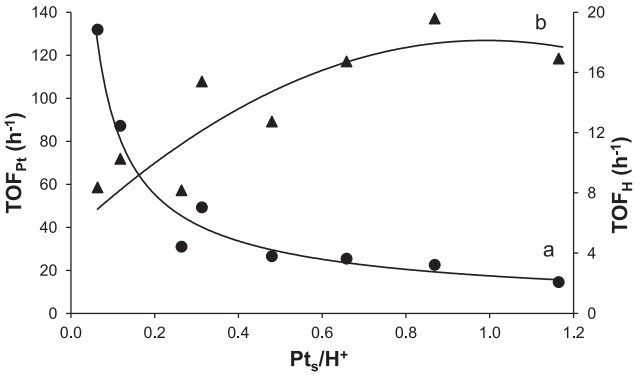

Fig. 5. Plot of TOF_{Pt} (a) and TOF_H (b) for *n*-hexane isomerisation over Pt/CsPW (0.20 g) versus atomic ratio of Pt_s and H^+ surface sites: 200 °C, 5.78 kPa *n*-hexane partial pressure in H_2 flow (20 mL min^{-1}), 5 h time on stream.

higher than that usually found for Pt/zeolite catalysts, which can be attributed to the stronger acidity of CsPW compared to the conventional zeolites.

The apparent activation energy, E_a, for *n*-hexane isomerisation over 5.78%Pt/CsPW was found to be 79 kJ mol^{-1} in the temperature range of 180–220 °C. The Arrhenius plot is shown in Fig. 6; in this plot, the differential conversion of *n*-hexane *X* which is directly proportional to the reaction rate is used. The high E_a value obtained indicates no diffusion limitations in the isomerisation reaction over Pt/CsPW.

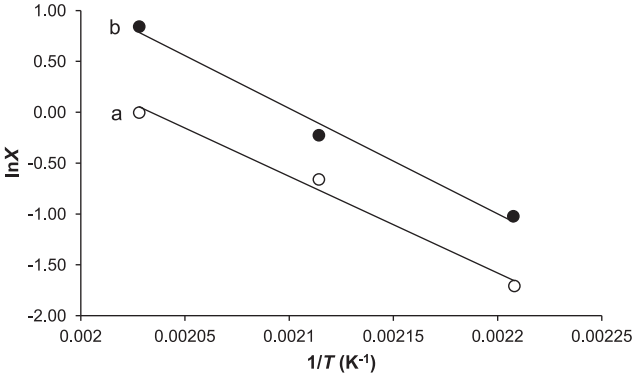

Fig. 6. Arrhenius plot for *n*-hexane isomerisation: (a) 5.78%Pt/CsPW (0.04 g) + SiO_2 (0.16 g) (E_a = 79 kJ mol^{-1}); (b) 5.57%Pt/4.25%Au/CsPW (0.04 g) + SiO_2 (0.16 g) (E_a = 86 kJ mol^{-1}); 5.78 kPa *n*-hexane partial pressure in H_2 flow (20 mL min^{-1}), 6 h time on stream.

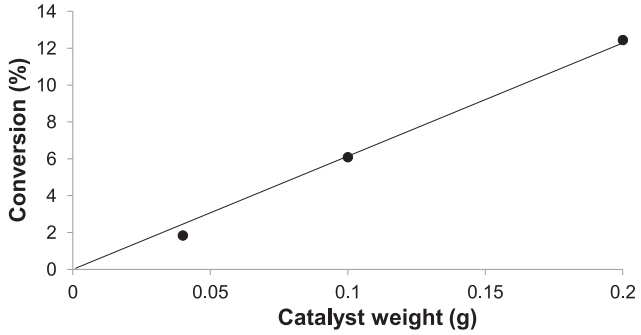

Fig. 7. Plot of *n*-hexane conversion versus catalyst weight: 5.87%Pt/CsPW diluted with SiO_2 to 0.20 g, 200 °C, 5.78 kPa *n*-hexane partial pressure in H_2 flow (20 mL min^{-1}), 6 h time on stream.

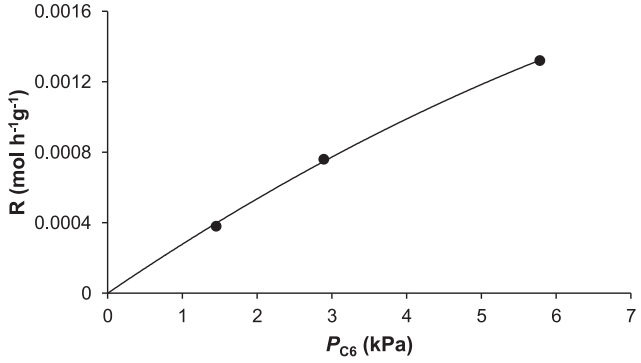

Fig. 8. Plot of reaction rate versus *n*-hexane partial pressure: 5.87%Pt/CsPW (0.04 g) + SiO_2 (0.16 g), 200 °C, 20 mL min^{-1} flow rate, 6 h time on stream, P_{H2} = 94–98 kPa (reaction order in *n*-hexane 0.90).

The isomerisation reaction is first order in Pt/CsPW catalyst (Fig. 7). The order in *n*-hexane was found to be 0.90 in agreement with Eq. (1) (Fig. 8, where P_{C6} is varied at practically constant P_{H2}). Also in accordance with Eq. (1), the reaction rate increases with increasing the partial pressure ratio P_{C6}/P_{H2}; 4-fold increase in P_{C6}/P_{H2} caused a factor of 1.5–1.8 increase in reaction rate for Pt/CsPW catalysts at 180 °C (Table 5). Overall, these kinetic results are in good agreement with Eq. (1), taking into account that in these reaction systems *n*-hexane dehydrogenation step was not always fully equilibrated.

3.3. Effect of gold

It has been well documented that bimetallic PtAu and PdAu catalysts frequently have an enhanced performance in comparison to monometallic Pt and Pd catalysts ([15,23–32] and references therein), for example in hydrogenation [32], hydrodeoxygenation [15,24], hydrodesulphurisation [30,31], oxidation [25–27] and other reactions (for review, see [23,28,29]). The enhancement of catalyst performance by addition of gold can be attributed to geometric (ensemble) and electronic (ligand) effects of the constituent elements in PtAu and PdAu bimetallic species [28,29].

A wide range of bimetallic catalysts have been studied in alkane and cycloalkane reactions such as hydrogenolysis, isomerisation, cyclisation, ring enlargement, etc., dating back to the 1970s [33–40]; these include both supported and alloy film PtAu and PdAu catalysts [33,36,37,39,40]. A short communication by Fraissard et al. [40] has reported the use of PtAu nanoparticles supported on zeolites (HY and HZSM-5) for hydroisomerisation of *n*-hexane. It has been found that 1%Pt/0.2%Au/HY and 1%Pt/HY have the same activity and selectivity in this reaction without any Au enhance-

Table 5
Effect of P_{C6}/p_{H2} partial pressure ratio.[a]

Catalyst	P_{C6}/P_{H2}	Conversion[b] %	10^3 R^c mol g^{-1} h^{-1}	TOF_{Pt}[d] h^{-1}
0.32%Pt/CsPW	0.061	3.89	0.39	24
0.32%Pt/CsPW	0.24	2.50	0.72	44
5.78%Pt/CsPW	0.061	7.95	0.98	3.3
5.78%Pt/CsPW	0.24	4.11	1.5	5.1
0.28%Pt/0.35%Au/CsPW	0.061	6.55	0.77	54
0.28%Pt/0.35%Au/CsPW	0.24	3.86	1.4	96
5.57%Pt/4.25%Au/CsPW	0.061	10.2	1.3	4.6
5.57%Pt/4.25%Au/CsPW	0.24	7.11	2.5	8.6

[a] 180 °C, 0.20 g catalyst, 20 mL min^{-1} flow rate.
[b] Average conversion over 6 h time on stream (mean of two parallel runs).
[c] Reaction rate calculated from $R = XF/W$, where X is the fractional conversion of n-hexane with the contribution of CsPW (0.012 and 0.010 at $P_{C6}/P_{H2} = 0.061$ and 0.24, respectively) subtracted, W is the catalyst weight (0.20 g) and F is the molar flow rate of n-hexane ($W/F = 20.8$ and 69.2 g h mol^{-1} at $P_{C6}/P_{H2} = 0.24$ and 0.061, respectively).
[d] Turnover frequency per surface Pt_s site with CsPW contribution subtracted.

ment; 1%Pt/0.2%Au/HZSM-5 shows good performance stability, but has not been tested against its Pt-only analogue.

Here we looked at the effect of Au additives on the performance of Pt/CsPW catalysts in the isomerisation of *n*-hexane. In this work, supported bimetallic catalysts PtAu/CsPW were prepared by co-impregnation of platinum and gold precursors onto CsPW followed by reduction of solid pre-catalysts with H_2 at 250 °C. This method would favour the formation of supported PtAu nanoparticles of a random composition together with various Pt and Au nanoparticles, rather than more uniform bimetallics that can be prepared in solution [29]. Information about the PtAu/CsPW catalysts studied (catalyst texture and metal dispersion) is given in Table 2.

STEM-EDX analysis indicated the presence of bimetallic nanoparticles in the PtAu/CsPW catalysts. The high-angle annular dark field (HAADF) STEM images of 5.78%Pt/CsPW, 2.62%Au/CsPW and 5.57%Pt/4.25%Au/CsPW catalysts are shown in Fig. 9, with metal nanoparticles indicated as bright spots on the darker background. These STEM images are difficult to analyse due to W, Pt and Au having similar large atomic numbers *Z* (74, 78, and 79, respectively). CsPW containing 70 wt% of W displays a strong background which makes it difficult to distinguish smaller Pt and Au particles from the *Z*-contrast HAADF images and determine accurately metal particle size distribution. Nevertheless, in Fig. 9a (5.78%Pt/CsPW catalyst), one can see platinum particles of $\leq$12 nm in size. The image of 2.62%Au/CsPW (Fig. 9b) shows oval shaped gold particles sized up 4–25 nm, with an average gold particle size $\leq$10 nm. Particles of a similar size and shape can be also seen in Fig. 9c (5.57%Pt/4.25%Au/CsPW), which indicates a PtAu alloying on the catalyst surface (see EDX analysis below).

The EDX analysis of a large number of metal nanoparticles in the 5.57%Pt/4.25%Au/CsPW catalyst showed that all these particles contained both Pt and Au in Pt/Au atomic ratios varying from 0.5 to 7.7 (Figs. S4 and S5). EDX elemental mapping (Fig. S6) shows that Pt and Au maps cover the same areas of PtAu/CsPW catalyst particles, indicating formation of a non-uniform PtAu particles (alloys), with local variations in Pt/Au atomic ratio.

Fig. 10a shows the XRD patterns of 5.57%Pt/4.25%Au/CsPW and 5.78%Pt/CsPW catalysts, in which the bcc pattern of crystalline CsPW [41] is dominated. Also clearly seen is the fcc pattern of Pt (39.8° [1 1 1] and 46.2° [2 0 0]) and Au (38.2° [1 1 1] and 44.4° [2 0 0]) metal nanoparticles. This confirms coexistence of Pt and Au particles in the PtAu/CsPW catalyst. In addition, PtAu bimetallic particles may be present with diffraction pattern falling in between the corresponding diffractions of the pure metals [29], which is obscured by the intense pattern of CsPW. Indeed, the close-up normalized difference XRD (Fig. 10b) shows a broad [1 1 1] diffraction peak in the range of 38–40° and possibly a weaker [2 0 0] peak in the range 44–46° between the diffractions of pure Pt and Au, which could be attributed to PtAu alloys. In Fig. 10a, the Pt peaks appear notably broader than the Au peaks, indicating higher dispersion of Pt particles. Although accurate analysis of metal particle size is difficult due to the prevailing CsPW pattern, rough estimate from the [1 1 1] peaks using the Scherrer equation gave 60 and 30 nm volume-average particle size for Au and Pt, respectively. This estimate, however, may be biased towards larger metal particles.

Representative results of PtAu/CsPW catalyst testing are shown in Table 4. Addition of gold to the Pt/CsPW catalysts was found to increase *n*-hexane conversion by a factor of 1.3–1.7 (Table 4, cf. entry 3 with 7 and 5 with 8), although the Au alone without Pt was inert (cf. entries 9 and 10 with 1). The effect of gold cannot be attributed to any change in Pt dispersion because Au additives practically did not change the dispersion of Pt in these catalysts (Table 2).

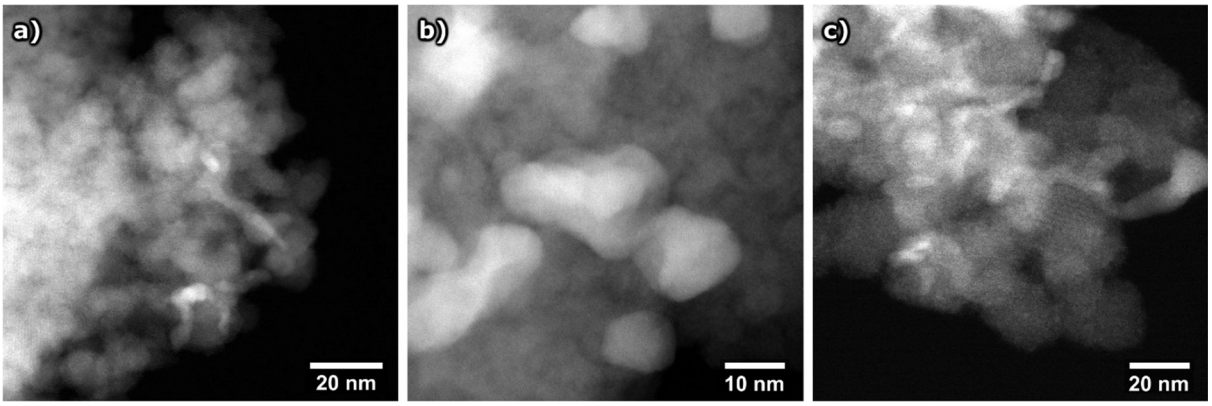

Fig. 9. HAADF-STEM images of (a) 5.78%Pt/CsPW, (b) 2.62%Au/CsPW and (c) 5.57%Pt/4.25%Au/CsPW catalysts, showing noble metal nanoparticles as bright spots.

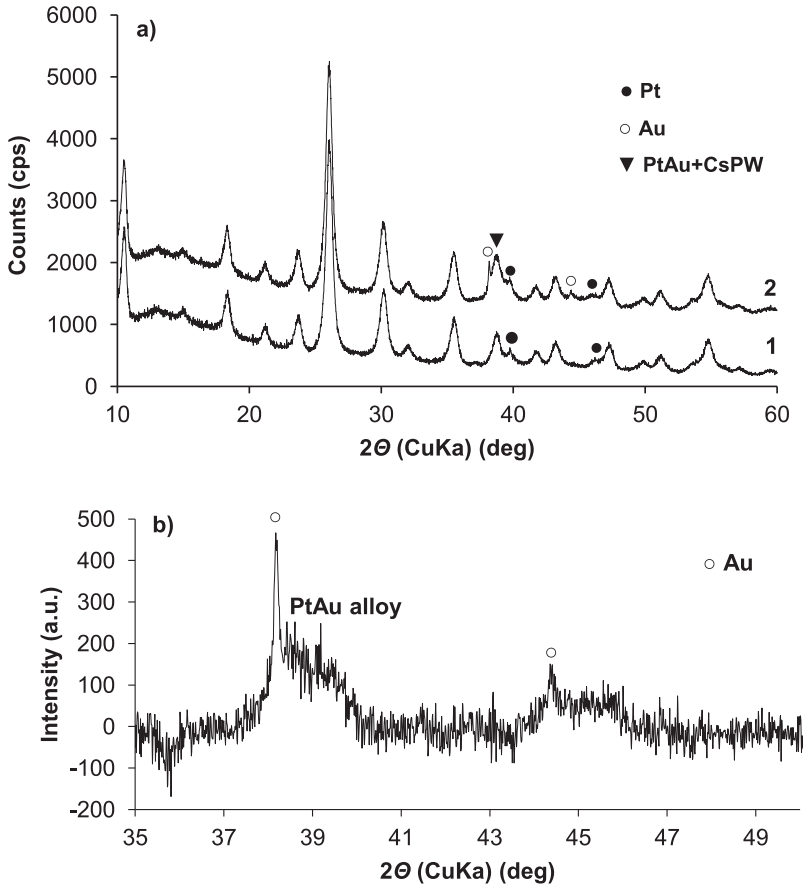

Fig. 10. Powder XRD patterns: (a) 5.78%Pt/CsPW (1) and 5.57%Pt/4.25%Au/CsPW (2); (b) close-up normalized difference (2)-(1) XRD pattern showing a broad [1 1 1] fcc PtAu alloy peak in the range 38–40° and possibly a weaker [2 0 0] PtAu alloy peak in the range 44–46°.

As seen from Table 4, gold additives, while increasing the conversion, did not affect reaction selectivity. This indicates that the effect of gold is pertinent to the Pt-catalysed dehydrogenation reaction step and does not affect subsequent reactions of carbenium ions (Scheme 2). It is important that the scale of Au effect on catalyst activity depended on the Pt loading, i.e., on the degree of equilibration of the dehydrogenation reaction step. Subtracting the contribution of CsPW (entry 1) from the conversion values in entries 3, 5, 7 and 8 gives the Au enhancement scale of a factor of 2.0 at a low Pt loading (~0.3%) and only a factor of 1.3 at a higher loading (~6%). This implies that the effect of Au is the strongest when alkane dehydrogenation is the rate-limiting step and decreases as alkane dehydrogenation approaches equilibrium.

Figs. 11 and 12 show comparative time courses for PtAu/CsPW versus Pt/CsPW and Au/CsPW versus CsPW, respectively, with *n*-hexane conversion and product selectivity as a function of the time on stream. Practically no coke was found in spent PtAu/CsPW catalysts, although a small amount of coke (0.3% C) was formed in Au/CsPW catalyst (Table S1). Nevertheless, the amount of coke in the Au/CsPW was less than that in CsPW (0.6%). This might explain a better performance stability of Au/CsPW compared to CsPW which can be seen in Fig. 12.

Kinetically, the reaction with PtAu/CsPW catalyst was found to be very similar to that with the monometallic Pt/CsPW described above. For PtAu/CsPW, the apparent activation energy was found to be 86 kJ mol^{-1} at 180–220 °C (cf. 79 kJ mol^{-1} for Pt/CsPW). As seen from the Arrhenius plot (Fig. 6), *n*-hexane conversion for the PtAu catalyst is higher than that for the Pt catalyst with very close Pt loading, thus conforming the Au enhancement in the whole temperature range. Similar to Pt/CsPW, the reaction with PtAu/CsPW is first order in the catalyst (Fig. S2) and 0.90 order in *n*-hexane (Fig. S3). Table 5 compares the effect of the P_{C6}/P_{H2} ratio for the reaction with Pt/CsPW and PtAu/CsPW catalysts. In both cases, the reaction rate increases with increasing the P_{C6}/P_{H2} ratio (a factor of 1.8–1.9 for PtAu/CsPW and 1.5–1.8 for Pt/CsPW when the P_{C6}/P_{H2} ratio was increased from 0.061 to 0.24); this is in agreement with rate Eq. (1). These results show that the reaction with both catalysts fits well with this equation.

The values of TOF_{Pt} in Table 5 give a more accurate estimate of the scale of gold effect. As seen, the gold enhancement of TOF_{Pt} is a factor of 2.2–2.3 for the 0.28–0.32% Pt loading and 1.4–1.7 for the 5.57–5.78% Pt loading. Thus the enhancing effect of gold decreases with increasing the Pt loading as *n*-hexane dehydrogenation step approaches quasi-equilibrium. It can therefore be anticipated that when the dehydrogenation step is fully equilibrated, the effect of gold will be close to zero.

Therefore, the results obtained demonstrate that gold additives can increase the activity of Pt/CsPW bifunctional catalyst in hydroisomerisation of *n*-hexane, although the gold alone is not active. More specifically, gold increases the catalytic activity of Pt sites in alkane dehydrogenation step. When alkane dehydrogenation is the rate-limiting step, the enhancing effect on the isomerisation reaction is at its maximum. At such conditions the enhancement of the turnover rate at the Pt surface sites amounts to a factor of ≥2 as can be seen from the TOF_{Pt} values in Table 5. Conversely, the effect of gold decreases as the dehydrogenation step approaches quasi-equilibrium. As shown above, in *n*-hexane isomerisation over Pt/CsPW, the dehydrogenation step is equilibrated at a molar ratio of Pt and H^+ surface sites $Pt_s/H^+ \geq 0.8$, corresponding to a Pt loading ≥6%. As a result, the gold enhancement is

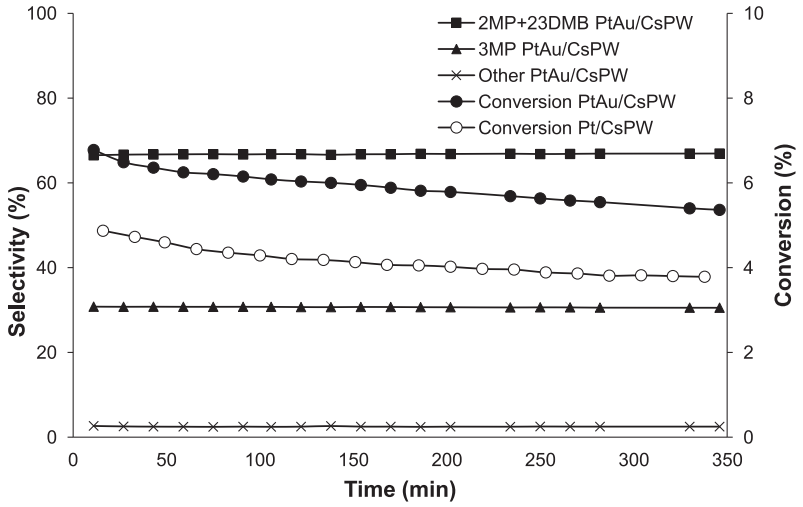

Fig. 11. *n*-Hexane isomerisation catalysed by 0.28%Pt/0.35%Au/CsPW (0.20 g) at 180 °C, 5.78 kPa *n*-hexane partial pressure in H_2 flow (20 mL min^{-1}). Open circles show *n*-hexane conversion with 0.32%Pt/CsPW catalyst at the same conditions; reaction selectivities are practically the same in both cases.

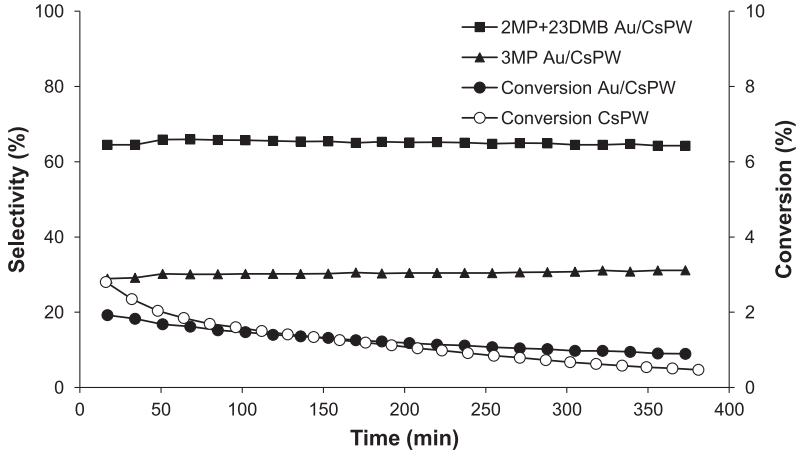

Fig. 12. *n*-Hexane isomerisation catalysed by 2.62%Au/CsPW (0.20 g) at 180 °C, 5.78 kPa *n*-hexane partial pressure, 20 mL min^{-1} H_2 flow rate. Open circles show *n*-hexane conversion with CsPW catalyst at the same conditions; reaction selectivities are practically the same in both cases.

observable at $Pt_s/H^+ < 0.8$ in this system. In the case of Pt-zeolite catalysts, the dehydrogenation step is equilibrated at $Pt_s/H^+ < 0.1$ [20,22], which is due to the weaker acid strength of zeolites compared to HPA. In this regard, the lack of gold enhancement in *n*-hexane isomerisation over 1%Pt/0.2%Au/HY as compared to 1%Pt/HY reported by Fraissard et al. [40] can be explained by equilibration of *n*-hexane dehydrogenation step in this system.

The nature of gold enhancement may be attributed to the previously documented electronic (ligand) and geometric (ensemble) effects in bimetallic PtAu species [28,29]. Our STEM-EDX analysis clearly indicates the presence of bimetallic PtAu nanoparticles in the PtAu/CsPW catalyst. The interaction between Pt and Au in these nanoparticles can lead to the superior catalyst performance in *n*-hexane isomerisation. Thorough structural characterisation of PtAu/CsPW catalyst complemented by computational studies may provide further insights into the gold effect in this system.

4. Conclusions

The isomerisation of *n*-hexane was carried out using acid and bifunctional metal-acid catalysts based on Keggin-type heteropoly acids at a gas-solid interface at 180–220 °C and ambient pressure in a fixed-bed microreactor. The bifunctional catalysts studied comprised Pt as the metal component and $Cs_{2.5}H_{0.5}PW_{12}O_{40}$ (CsPW), an acidic Cs salt of heteropoly acid $H_3PW_{12}O_{40}$, as the acid component. Addition of gold to the Pt/CsPW catalyst was found to increase the catalytic activity, although the Au alone without Pt was inert. The enhancement of catalyst performance is suggested to be caused by PtAu alloying. The STEM-EDX and XRD analyses of the PtAu/CsPW catalysts indicate the presence of bimetallic PtAu nanoparticles with a wide range of Pt/Au atomic ratios.

Acknowledgements

We thank Dr T. Heil from Nanoinvestigation Centre, University of Liverpool for assistance with the STEM. Dr D. Belic acknowledges funding through ERC Advanced Grant "PANDORA" No. 108269.

Appendix A. Supplementary material

Supplementary data associated with this article can be found, in the online version, at https://doi.org/10.1016/j.jcat.2017.11.001.

References

[1] L. Lloyd, Handbook of Industrial Catalysts, Fundamental and Applied Catalysis, Springer, 2011, pp. 256–258.
[2] H. Matsuhashi, H. Shibata, H. Nakamura, K. Arata, Appl. Catal. A 187 (1999) 99–106.
[3] S.T. Sie, in: G. Ertl, H. Knözinger, F. Schüth, J. Weitkamp (Eds.), Handbook of Heterogeneous Catalysis, vol. 1, Wiley-VCH, 2008, p. 2809.
[4] , Advances in Catalysis and Related Subjects vol. 13 (1963) 157.
[5] A. Miyaji, T. Echizen, L. Li, T. Suzuki, Y. Yoshinaga, T. Okuhara, Catal. Today 74 (2002) 291–297.
[6] T. Okuhara, N. Mizuno, M. Misono, Adv. Catal. 41 (1996) 113–252.
[7] I.V. Kozhevnikov, Catalysis by Polyoxometalates, Wiley & Sons, Chichester, England, 2002.
[8] S.-S. Wang, G.-Y. Yang, Chem. Rev. 115 (2015) 4893–4962.
[9] A.V. Ivanov, T.V. Vasina, V.D. Nissenbaum, L.M. Kustov, M.N. Timofeeva, J.I. Houzvicka, Appl. Catal. A: Gen. 259 (2004) 65–72.
[10] W. Knaeble, R.T. Carr, E. Iglesia, J. Catal. 319 (2014) 283–296.
[11] T. Pinto, P. Arquillière, V. Dufaud, F. Lefebvre, Appl. Catal. A: Gen. 528 (2016) 44–51.
[12] F. Lefebvre, Curr. Catal. 6 (2017) 77–89.
[13] Y. Izumi, M. Ono, M. Kitagawa, M. Yoshida, K. Urabe, Micropor. Mater. 5 (1995) 255–262.
[14] K. Alharbi, W. Alharbi, E.F. Kozhevnikova, I.V. Kozhevnikov, ACS Catal. 6 (2016) 2067–2075.
[15] O. Poole, K. Alharbi, D. Belic, E.F. Kozhevnikova, I.V. Kozhevnikov, Appl. Catal. B: Environ. 202 (2017) 446–453.
[16] K. Alharbi, E.F. Kozhevnikova, I.V. Kozhevnikov, Appl. Catal. A 504 (2015) 457–462.
[17] J.E. Benson, M. Boudart, J. Catal. 4 (1965) 704–710.
[18] J.E. Benson, H.S. Hwang, M. Boudart, J. Catal. 30 (1973) 146–153.
[19] T. Pinto, V. Dufaud, F. Lefebvre, Appl. Catal. A: Gen. 483 (2014) 103–108.
[20] F. Ribeiro, C. Marcilly, M. Guisnet, J. Catal. 78 (1982) 267–274.
[21] A. van de Runstraat, J.A. Kamp, P.J. Stobbelaar, J. van Grondelle, S. Krijnen, R.A. van Santen, J. Catal. 171 (1997) 77–84.
[22] P.S.F. Mendes, F.M. Mota, J.M. Silva, M.F. Ribeiro, A. Daudin, C. Bouchy, Catal. Sci. Technol. 7 (2017) 1095–1107.
[23] G.J. Hutchings, Chem. Commun. (2008) 1148–1164.
[24] K. Sun, A.R. Wilson, S.T. Thompson, H.H. Lamb, ACS Catal. 5 (2015) 1939–1948.
[25] Y.F. Han, J.H. Wang, D. Kumar, Z. Yan, D.W. Goodman, J. Catal. 232 (2005) 467–475.
[26] E.K. Hanrieder, A. Jentys, J.A. Lercher, J. Catal. 333 (2016) 71–77.
[27] J. Xu, T. White, P. Li, C. He, J. Yu, W. Yuan, Y.F. Han, J. Am. Chem. Soc. 132 (2010) 10398–10406.
[28] B. Coq, F. Figueras, J. Mol. Catal. A: Chem. 173 (2001) 117–134.
[29] F. Gao, D.W. Goodman, Chem. Soc. Rev. 41 (2012) 8009–8020.
[30] A.M. Venezia, V. La Parola, V. Nicoli, G. Deganello, J. Catal. 212 (2002) 56–62.
[31] A.M. Venezia, V. La Parola, G. Deganello, B. Pawelec, J.L.G. Fierro, J. Catal. 215 (2003) 317–325.
[32] T.J. Schwartz, S.D. Lyman, A.H. Motagamwala, M.A. Mellmer, J.A. Dumesic, ACS Catal. 6 (2016) 2047–2054.
[33] J.R.H. van Schaik, R.P. Dessing, V. Ponec, J. Catal. 38 (1975) 273–282.
[34] Z. Karpinski, J.K.A. Clarke, J. Chem. Soc., Faraday Trans. 1 (71) (1975) 2310–2318.
[35] J.K.A. Clarke, A.F. Kane, T. Baird, J. Catal. 64 (1980) 200–212.
[36] A.F. Kane, J.K.A. Clarke, J. Chem. Soc., Faraday Trans. I (76) (1980) 1640–1651.
[37] J.K.A. Clarke, A.C.M. Creaner, T. Baird, Appl. Catal. 9 (1984) 85–108.
[38] Z. Karpinski, W. Juszczyk, J. Stachurski, J. Chem. Soc., Faraday Trans. 1 (81) (1985) 1447–1454.
[39] B.D. Chandler, A.B. Schabel, L.H. Pignolet, J. Catal. 193 (2000) 186–198.
[40] J. Fraissard, V. Gerda, K.I. Patrylak, Yu.G. Voloshyna, Catal. Today 122 (2007) 338–340.
[41] T. Okuhara, H. Watanabe, T. Nishimura, K. Inumaru, M. Misono, Chem. Mater. 12 (2000) 2230–2238.